IEEE Access
Multidisciplinary | Rapid Review | Open Access Journal

Received August 30, 2018, accepted October 1, 2018, date of publication October 5, 2018, date of current version October 29, 2018.

Digital Object Identifier 10.1109/ACCESS.2018.2874010

Quadratic Taylor Approximation Demosaicking System Using Post-Processing for Zipper Artifact Removal

DAEJUN PARK AND JECHANG JEONG, (Member, IEEE)
Department of Electronics and Computer Engineering, Hanyang University, Seoul 04763, South Korea

Corresponding author: Jechang Jeong (jjeong@hanyang.ac.kr)

This work was supported by the ICT R&D Program of MSIP/IITP, Software Platform for ICT Equipment, under Grant 2014-0-00670.

ABSTRACT In this paper, we propose a new demosaicking system that uses post-processing technique to remove zipper artifacts that are primarily caused by improper interpolation in a quincunx-sampled green plane. We use a high-order approximation to predict accurate pixel values in the weighted average-based green channel interpolation. We also perform prediction using a color difference model in the red and blue channel interpolation process. As a well-designed demosaicking system too cannot prevent the occurrence of ON–OFF pattern artifacts and the resulting false colors, we propose post-processing for zipper artifact detection and removal to improve the demosaicked image. After performing the just noticeable difference model-based zipper artifact detection in the luminance image of the demosaicked image, the clamping-based zipper artifact removal process is performed in the red, green, and blue planes. Experimental results demonstrate that the proposed demosaicking system improves both the objective and subjective image qualities compared to the conventional state-of-the-art demosaicking algorithms.

INDEX TERMS Color filter array interpolation, demosaicking, image processing, just noticeable difference.

I. INTRODUCTION

The majority of digital cameras use a single electronic sensor to acquire images [1]. Color filters are used to separate the color information of the incoming light. The color filters filter light into a wavelength range such that it produces a color filter array (CFA) image that separates information about the color of light [2]. For example, a Bayer filter [3] separates light information into three wavelength regions, red (R), green (G), and blue (B), as shown in Fig. 1. The G components with the highest sensitivity of human visual system (HVS) are sampled twice as much as the R/B components.

To reconstruct a full RGB image from CFA image, we interpolate the G components of quincunx grid and the R/B components of rectangular grid. This process is called the demosaicking process or CFA interpolation process [4]. The demosaicking process is performed using the property that the spatial and spectral correlations between neighboring pixels are high [5]–[10].

Over the years, several demosaicking techniques have been developed. A demosaicking technique using variance of color differences (VCD) [5] performs edge detection using variance of color differences. Effective demosaicking using subband correlation (EDUSC) [6] presented discrete wavelet transform to classify edge pixels. In [7], Pekkucuksen and Altunbasak proposed a CFA interpolation method using an orientation-free edge strength filter (ESF). Effective demosaicking algorithm based on edge property (EDAEP) [8] was

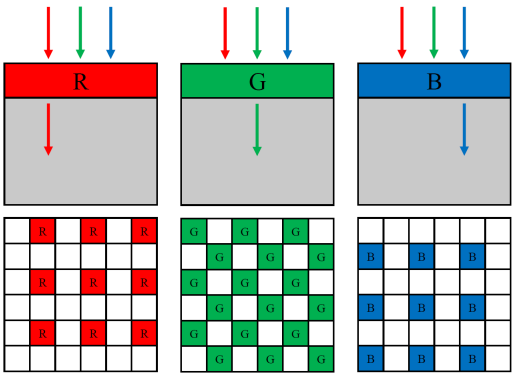

FIGURE 1. Example of a Bayer filter.

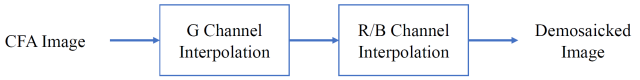

FIGURE 2. Flowchart of the CFA interpolation algorithm.

proposed to remove color artifacts using improved effective color interpolation. Dengwen *et al.* [9] proposed color demosaicking with directional filtering and weighting (CDDFW) by combining directional filtering and a posteriori decision technique with enhanced effective color interpolation. Chen *et al.* [10] proposed a voting-based directional interpolation (VDI) method to combine voting-based edge direction detection with weighting-based interpolation.

Several developers have tried to eliminate the demosaicking artifacts, such as zipper artifacts [11], which are inevitably generated in the interpolation process, by using post-processing for increasing interpolation accuracy or for performing repetitive interpolation for accurate color prediction. Adaptive homogeneity-directed (AHD) demosaicking method [12] applies median filtering to color differences to suppress small variations in color while preserving edges. In the demosaicking method using the high-order interpolation technique (HOI) proposed by Li and Randhawa [13], a weighted median filtering is used to produce an output based on the edge orientation map. Though these attempts increased the interpolation accuracy in the smooth and strong edge regions, they failed to remove the noticeable zipper artifacts. Despite numerous demosacking algorithms being developed, artifacts still remain in thin lines, object boundaries, and so on.

We refer to the on-off pattern artifacts as zipper artifacts and intend to detect and eliminate them. Just noticeable difference (JND) model-based artifact detection is performed on a luminance image of a demosaicked full RGB image. For artifact removal, we performed color pixel value clamping in the RGB domain. In accordance with the sampling grid of the Bayer pattern, we determined the minimum and maximum values of surrounding original pixel values and clamped the interpolated pixel values. This eliminates artifacts of the on-off pattern.

The remainder of this paper is organized as follows. In section II, we introduced the interpolation technique used in the proposed demosaicking system. In section III, we addressed the JND model-based artifact detection process and the clamping-based artifact removal process. In section IV, we conducted the experiments and presented the results. Finally, we concluded the paper in section V.

II. SECOND-ORDER TAYLOR APPROXIMATION-BASED CFA INTERPOLATION

Considering the complexity of the postproceeing proposed in this paper, we use a relatively simple CFA interpolation technique. Fig. 2 presents a flowchart of the demosaicking technique based on the second-order Taylor approximation. After performing the interpolation of the G component at the R/B pixel positions, the interpolation of the remaining color planes is performed using the color difference model [14]. As the R/B sampling components have similar conditions, only the demosaicking technique related to the R pixel position is described.

A. GREEN CHANNEL RECONSTRUCTION

As the spectral and spatial correlations between surrounding pixels are high, missing G values are obtained by weighted averaging of the four directional G values. By determining the weight values and the predictors using the second derivatives for the north (N), south (S), west (W), and east (E) directions, we can reconstruct the G plane using (1).

$$\hat{G} = \frac{w_N G_N + w_S G_S + w_W G_W + w_E G_E}{w_N + w_S + w_W + w_E}. \tag{1}$$

where w_N, w_S, w_W, and w_E are the inverse gradient weight values in the N, S, W, and E directions, respectively. G_N, G_S, G_W, and G_E are predictors for each direction.

$$\begin{aligned} d_N = {} & |R_{i+2,j} - 2R_{i,j} + R_{i-2,j}| \\ & + |R_{i,j} - 2R_{i-2,j} + R_{i-4,j}| \\ & + |G_{i+1,j} - 2G_{i-1,j} + G_{i-3,j}| \\ & + |G_{i,j-1} - 2G_{i-2,j-1} + G_{i-4,j-1}|/2 \\ & + |G_{i,j+1} - 2G_{i-2,j+1} + G_{i-4,j+1}|/2, \end{aligned} \tag{2}$$

$$\begin{aligned} d_S = {} & |R_{i-2,j} - 2R_{i,j} + R_{i+2,j}| \\ & + |R_{i,j} - 2R_{i+2,j} + R_{i+4,j}| \\ & + |G_{i-1,j} - 2G_{i+1,j} + G_{i+3,j}| \\ & + |G_{i,j-1} - 2G_{i+2,j-1} + G_{i+4,j-1}|/2 \\ & + |G_{i,j+1} - 2G_{i+2,j+1} + G_{i+4,j+1}|/2, \end{aligned} \tag{3}$$

$$\begin{aligned} d_W = {} & |R_{i,j+2} - 2R_{i,j} + R_{i,j-2}| \\ & + |R_{i,j} - 2R_{i,j-2} + R_{i,j-4}| \\ & + |G_{i,j+1} - 2G_{i,j-1} + G_{i,j-3}| \\ & + |G_{i-1,j} - 2G_{i-1,j-2} + G_{i-1,j-4}|/2 \\ & + |G_{i+1,j} - 2G_{i+1,j-2} + G_{i+1,j-4}|/2, \end{aligned} \tag{4}$$

$$\begin{aligned} d_E = {} & |R_{i,j-2} - 2R_{i,j} + R_{i,j+2}| \\ & + |R_{i,j} - 2R_{i,j+2} + R_{i,j+4}| \\ & + |G_{i,j-1} - 2G_{i,j+1} + G_{i,j+3}| \\ & + |G_{i-1,j} - 2G_{i-1,j+2} + G_{i-1,j+4}|/2 \\ & + |G_{i+1,j} - 2G_{i+1,j+2} + G_{i+1,j+4}|/2. \end{aligned} \tag{5}$$

where d_N, d_S, d_W, and d_E in (2)-(5) are gradient values based on the second-order derivatives. The reference pixels grid used to calculate the N gradient value for a given R pixel position is shown in Fig. 3. The inverse gradient weights in each direction are presented in the following equations.

$$\begin{aligned} w_N &= \frac{1}{1+d_N}, \quad w_S = \frac{1}{1+d_S}, \\ w_W &= \frac{1}{1+d_W}, \quad w_E = \frac{1}{1+d_E}. \end{aligned} \tag{6}$$

where the value '1' is added to the denominator to prevent it from being divided by zero. In general, the area where

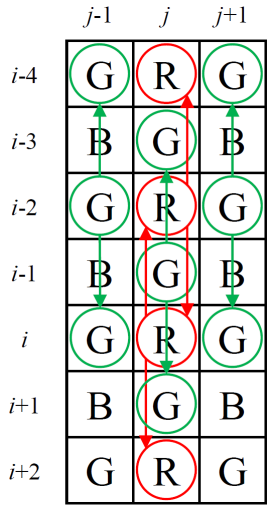

FIGURE 3. The reference pixels used to determine d_N in (2).

artifacts occur has a large color gradient and a small weight value.

We adopt Taylor series in the G channel interpolation process. The general form of Taylor series is given by

$$f(x) = f(a) + \frac{f'(a)}{1!}(x-a) + \frac{f''(a)}{2!}(x-a)^2 + \cdots. \quad (7)$$

We use the quadratic Taylor approximation to determine four directional predictors, as shown in (8)-(11).

$$G_N = G_{i-1,j} + G'_N + \frac{1}{2!}G''_N, \quad (8)$$

$$G_S = G_{i+1,j} + G'_S + \frac{1}{2!}G''_S, \quad (9)$$

$$G_W = G_{i,j-1} + G'_W + \frac{1}{2!}G''_W, \quad (10)$$

$$G_E = G_{i,j+1} + G'_E + \frac{1}{2!}G''_E. \quad (11)$$

where G'_D and G''_D are the first and second-order derivative values for the D direction, respectively.

$$G'_N = \frac{g_{i,j} - g_{i-2,j}}{i-(i-2)} \cong \frac{R_{i,j} - R_{i-2,j}}{2}, \quad (12)$$

$$\begin{aligned} G''_N &\cong \frac{R''_{i,j} + R''_{i-2,j}}{2} \\ &= \frac{1}{2}\left(\frac{R_{i-2,j} - 2R_{i,j} + R_{i+2,j}}{4} + \frac{R_{i-4,j} - 2R_{i-2,j} + R_{i,j}}{4}\right) \\ &= \frac{R_{i-4,j} - R_{i-2,j} - R_{i,j} + R_{i+2,j}}{8}. \end{aligned} \quad (13)$$

Using (12) and (13), we can obtain the first and second-order derivative values for the N direction. We assume that the color planes exhibit the similar high frequency characteristics, and replace the missing G pixel information at the chroma pixel location with the R/B pixel information. By including the second-order derivative value in the prediction, more detail components can be considered [6], [7], [9]. Similarly, the derivative values can be obtained for the S, W, and E directions. Finally, the G channel ($\hat{G}$) is reconstructed using the weighted average method of (1).

B. RED AND BLUE CHANNEL INTERPOLATION

After $\hat{G}$ plane is obtained, interpolation of the R/B components is performed. In the R/B interpolation process in the B/R pixel position, we describe only the B interpolation at the R pixel location. The weighted average method in (14) and (15) is performed using the color differences between the original B and $\hat{G}$ components, which exist in the diagonal directions, northwest (NW), southwest (SW), northeast (NE), and southeast (SE).

$$\hat{B}_{i,j} = \hat{G}_{i,j} + \tilde{C}_{BG}, \quad (14)$$

$$\tilde{C}_{BG} = \frac{w_{NW}C_{NW} + w_{SW}C_{SW} + w_{NE}C_{NE} + w_{SE}C_{SE}}{w_{NW} + w_{SW} + w_{NE} + w_{SE}}. \quad (15)$$

where w_{NW}, w_{SW}, w_{NE}, and w_{SE} are the inverse gradient weight values in the NW, SW, NE, and SE directions, respectively. $\tilde{C}_{BG}$ is the weghted average value of color differences C_{NW}, C_{SW}, C_{NE}, and C_{SE}.

Equations (16)-(19) are used to calculate the directional gradients d_{NW}, d_{SW}, d_{NE}, and d_{SE}.

$$d_{NW} = \left|B_{i-1,j-1} - \hat{G}_{i-1,j-1}\right|, \quad (16)$$

$$d_{SW} = \left|B_{i+1,j-1} - \hat{G}_{i+1,j-1}\right|, \quad (17)$$

$$d_{NE} = \left|B_{i-1,j+1} - \hat{G}_{i-1,j+1}\right|, \quad (18)$$

$$d_{SE} = \left|B_{i+1,j+1} - \hat{G}_{i+1,j+1}\right|. \quad (19)$$

The weights of (20) are obtained by the determined gradient values.

$$w_{NW} = \frac{1}{1+d_{NW}}, \quad w_{SW} = \frac{1}{1+d_{SW}}, \quad w_{NE} = \frac{1}{1+d_{NE}}, \quad w_{SE} = \frac{1}{1+d_{SE}}. \quad (20)$$

The color differences C_{NW}, C_{SW}, C_{NE}, and C_{SE} are given by the following:

$$C_{NW} = B_{i-1,j-1} - \hat{G}_{i-1,j-1}, \quad (21)$$

$$C_{SW} = B_{i+1,j-1} - \hat{G}_{i+1,j-1}, \quad (22)$$

$$C_{NE} = B_{i-1,j+1} - \hat{G}_{i-1,j+1}, \quad (23)$$

$$C_{SE} = B_{i+1,j+1} - \hat{G}_{i+1,j+1}. \quad (24)$$

We can interpolate the R/B channels at the G pixel positions using (25) and (26).

$$\hat{R}_{i,j} = G_{i,j} + \frac{1}{2}(R_{i,j-1} - \hat{G}_{i,j-1} + R_{i,j+1} - \hat{G}_{i,j+1}), \quad (25)$$

$$\hat{B}_{i,j} = G_{i,j} + \frac{1}{2}(B_{i-1,j} - \hat{G}_{i-1,j} + B_{i+1,j} - \hat{G}_{i+1,j}). \quad (26)$$

III. POST-PROCESSING FOR ZIPPER ARTIFACT DETECTION AND REMOVAL

Demosaicking artifacts are primarily caused by inaccurate selection of reference pixels in the interpolation process.

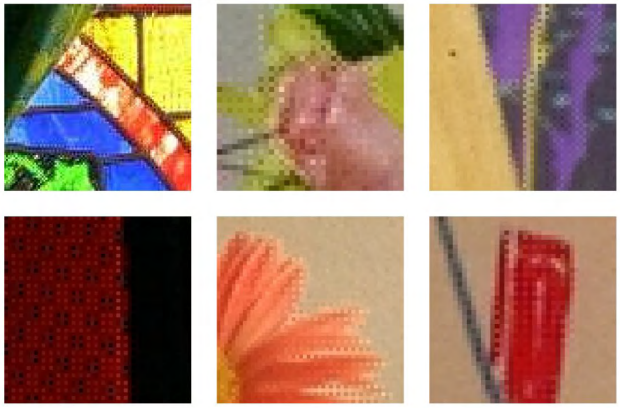

FIGURE 4. Examples of zipper artifacts.

A better predictor tends to select a larger number of reference pixels in the prediction process, leading to a large size kernel to be used in the interpolation process. In this case, zipper artifacts, as shown in Fig. 4, are inevitably generated at thin lines and object boundaries.

There are two steps in the proposed post-processing for eliminating zipper artifacts. First, JND model-based zipper artifact detection is performed on the luminance image, after which clamping-based artifact removal is performed. Fig. 5 illustrates a flowchart of the post-processing part used in the proposed demosaicking system.

A. LUMINANCE IMAGE GENERATION

Luminance (L) is the luminous intensity that indicates how bright an object appears to the HVS. An achromatic component L contains information about the spatial resolution of the image. We express L as a weighted sum of R, G, and B as in (27).

$$L = 0.2126R + 0.7152G + 0.0722B. \tag{27}$$

where R, G, and B components are assumed to be linear.

B. JND MODEL

The HVS is known to be unable to distinguish any changes below the JND threshold around a pixel because of their underlying spatial/temporal sensitivity and masking properties. We use these properties to perform artifact detection in the post-processing.

In this paper, we used the JND predictor of the pixel domain for luminance image. Luminance adaptation (LA) and contrast masking (CM) are the major considerations for the spatial JND. LA refers to the masking effect of the HVS toward background luminance, while CM denotes the visibility reduction of one visual signal in the presence of another one and includes edge masking (EM) and texture masking (TM).

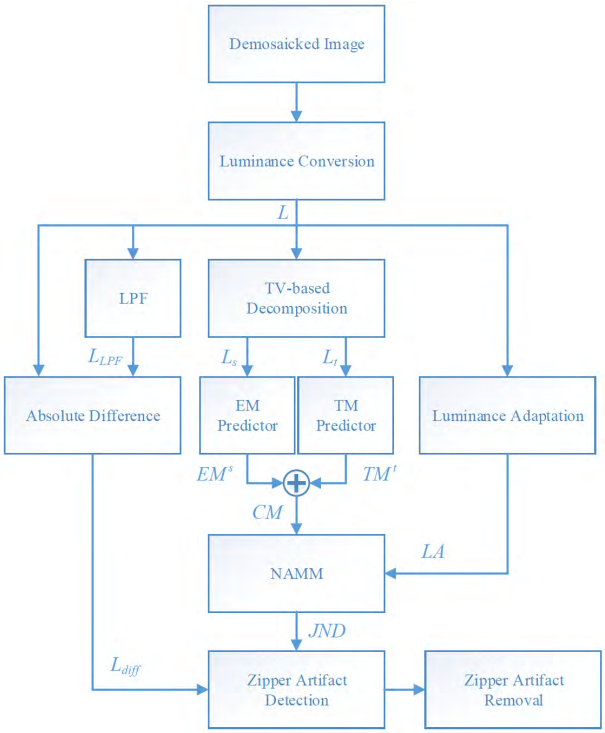

FIGURE 5. Flowchart of the post-processing used in the proposed demosaicking system.

The formula for LA [15] is as follows.

$$LA_{i,j} = \begin{cases} 17 \times (1 - \sqrt{\bar{L}_{i,j}/127}) + 3, & if\ \bar{L}_{i,j} \le 127, \\ 3 \times (\bar{L}_{i,j} - 127)/128 + 3, & otherwise. \end{cases} \tag{28}$$

where $\bar{L}_{i,j}$ is the 5×5 mean luminance value at (i, j) position.

For the calculation of CM, we obtain the structural image L_s and the textural image L_t through an image decomposition process. For efficient separation, we used a total variation-based image decomposition model [16]. Here, CM is given as follows.

$$CM_{i,j} = EM^s_{i,j} + TM^t_{i,j}, \tag{29}$$

$$\begin{cases} EM^s_{i,j} = SC^s_{i,j} \cdot \beta \cdot W_s \\ TM^t_{i,j} = SC^t_{i,j} \cdot \beta \cdot W_t \end{cases} \tag{30}$$

where EM^s and TM^t are the EM of the structural image L_s and TM of the textural image L_t, respectively. SC is the maximum luminance difference within the 5×5 neighborhood. W_s and W_t are the contributions of EM and TM to the CM, which are set to 1 and 3, respectively. β is set to 0.017.

Non-linear additivity model for masking (NAMM) is used to determine the visibility threshold for overall masking effect. Integration of LA and CM for overall JND estimation is presented in the following equation.

$$JND_{i,j} = LA_{i,j} + CM_{i,j} - \alpha \cdot min(LA_{i,j}, CM_{i,j}). \tag{31}$$

where α is the gain reduction factor in NAMM because of overlapping between two masking factors. α is set to 0.3.

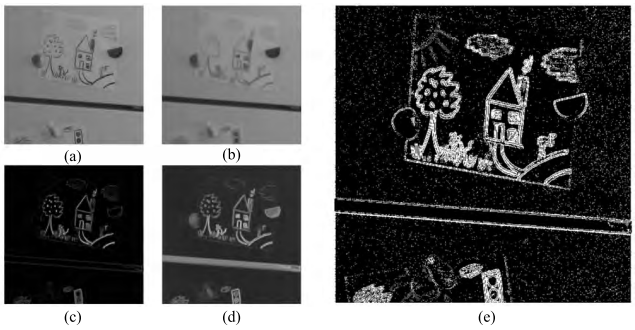

FIGURE 6. Examples of images used in the zipper artifact detection process (a) luminance image, (b) low-pass filtered luminance image, (c) luminance difference image, (d) JND map, and (e) zipper artifact map.

C. ZIPPER ARTIFACT DETECTION

Detection of the zipper artifact is performed by comparing the L_{diff} image, which is the difference between the luminance image L and the low-pass filtered luminance image L_{LPF}, and the JND derived from section III-B. L_{diff} is obtained by (32) and (33).

$$L_{diff} = |L - L_{LPF}|, \tag{32}$$

$$L_{LPF} = L * h. \tag{33}$$

where h is a $k \times k$ Gaussian low-pass filter and $*$ is the convolution operator.

Fig. 6 presents the images used in the proposed zipper artifact detection process. Comparison of L_{diff} and JND helps determine the presence of artifacts in the image. If L_{diff} is greater than JND, it is seen that artifacts due to demosaicking (zipper artifacts) at the pixel location have occurred.

D. ZIPPER ARTIFACT REMOVAL

Median filtering is commonly used for the on-off pattern artifact removal. However, applying median filtering to an image that actually has an on-off pattern or texture region will result in another artifact as median filtering performs the mapping to the median value. Therefore, in this paper, artifact removal is performed through the clamping process in the color domain using the neighboring pixels' minimum and maximum values.

Fig. 7 illustrates the reference pixels used in the clamping process (34). At the R (B) position in Fig. 7(a) (Fig. 7(b)), the four surrounding G or B (R) components are used as candidates. In the G position, six pixels are used as candidates for clamping R or B, as shown in Fig. 7(c) and (d), respectively. The clamping process is determined as follows.

$$X' = \begin{cases} X_{min}, & if\ X < X_{min}, \\ X_{max}, & else\ if\ X > X_{max}, \\ X, & otherwise. \end{cases} \tag{34}$$

where $X \in \{\hat{R}, \hat{G}, \hat{B}\}$, X_{min} and X_{max} represent the minimum and maximum values of neighboring pixels, respectively. X' is the finally determined color component.

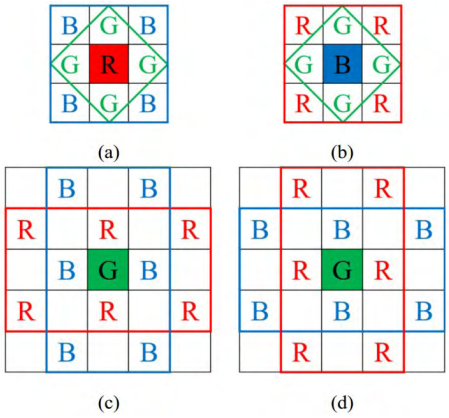

FIGURE 7. The reference pixels used in the clamping-based zipper artifact removal process at the (a) R, (b) B, (c) G1, and (d) G2 positions.

TABLE 1. McM dataset (500 × 500 in TIFF format).

TABLE 2. LC dataset (720 × 540 or 540 × 720 in TIFF format).

IV. EXPERIMENTAL RESULTS

In this section, we demonstrate the superiority of the proposed demosaicking system by comparing it with existing algorithms (VCD [5], EDUSC [6], ESF [7], EDAEP [8], CDDFW [9], and VDI [10]). In the subjective image quality evaluation process, the proposed post-processing technique is also compared with the AHD [12] and HOI [13] algorithms.

We used the McMaster (McM) dataset [17] shown in Table 1 to verify the objective performance of the proposed demosaicking system. In addition, Laurent Condat's (LC) Image Database [18] is used to evaluate the subjective performance of the proposed demosaicking system. McM and LC images have lower spectral correlations and are close to

TABLE 3. CPSNR results (dB) of conventional algorithms and proposed algorithm for McM dataset.

CPSNR	VCD	EDUSC	ESF	EDAEP	CDDFW	VDI	Proposed
1	34.7274	33.8434	33.4539	34.7038	34.7518	35.1791	35.3209
2	38.1614	37.2405	36.6402	38.2215	38.0609	38.6028	38.4825
3	36.9338	36.7852	36.3614	36.9606	37.1964	37.4923	37.2900
4	38.8667	38.2388	37.5863	38.8473	38.4622	40.5706	39.6844
5	37.9844	37.0668	36.5230	37.9571	37.9297	38.6618	38.9307
6	39.1931	37.3721	36.3321	39.1383	39.0690	40.1340	40.0148
7	40.4042	42.2561	41.9796	39.8758	41.1090	38.7783	38.9979
8	41.8291	41.5351	41.2262	41.4634	42.0450	41.3521	41.2104
9	39.3045	38.1986	37.6856	39.4681	39.2656	40.4541	40.2621
10	40.6224	39.1611	38.2706	40.6405	40.4358	41.1095	41.1310
11	41.4689	40.1076	39.3910	41.6193	41.5993	41.9505	42.0240
12	41.1848	39.9513	39.8139	41.4017	41.4790	41.8394	41.8172
13	42.8222	41.9454	41.2179	42.8563	42.8558	43.5430	43.8338
14	41.3530	40.6065	39.7822	41.4177	41.4400	41.9936	41.9621
15	41.2369	40.4078	39.7147	41.3366	41.1530	41.8771	41.8070
16	37.1661	36.1010	35.5167	37.3835	37.4388	37.7465	38.1131
17	36.1897	34.7277	34.3469	36.2680	35.9721	37.1455	36.9516
18	38.2171	37.1221	36.6941	38.2825	38.2715	38.4289	39.1763
Average	39.3148	38.4815	37.9187	39.3246	39.3631	39.8255	39.8339

TABLE 4. FSIMc results of conventional algorithms and proposed algorithm for McM dataset.

FSIMc	VCD	EDUSC	ESF	EDAEP	CDDFW	VDI	Proposed
1	0.99217	0.98922	0.98578	0.99251	0.99303	0.99364	0.99364
2	0.99643	0.99537	0.99402	0.99657	0.99670	0.99695	0.99670
3	0.99695	0.99702	0.99577	0.99718	0.99741	0.99698	0.99673
4	0.99813	0.99799	0.99698	0.99837	0.99833	0.99871	0.99835
5	0.99685	0.99536	0.99354	0.99697	0.99720	0.99768	0.99793
6	0.99820	0.99676	0.99430	0.99824	0.99838	0.99862	0.99868
7	0.99817	0.99878	0.99853	0.99808	0.99818	0.99722	0.99735
8	0.99781	0.99774	0.99688	0.99802	0.99797	0.99778	0.99743
9	0.99735	0.99655	0.99465	0.99754	0.99768	0.99803	0.99773
10	0.99836	0.99791	0.99697	0.99839	0.99856	0.99860	0.99865
11	0.99824	0.99790	0.99681	0.99838	0.99857	0.99844	0.99857
12	0.99826	0.99790	0.99717	0.99837	0.99836	0.99851	0.99866
13	0.99797	0.99733	0.99590	0.99804	0.99827	0.99857	0.99862
14	0.99809	0.99760	0.99671	0.99814	0.99836	0.99864	0.99848
15	0.99790	0.99769	0.99693	0.99796	0.99814	0.99822	0.99822
16	0.99714	0.99597	0.99288	0.99742	0.99765	0.99776	0.99764
17	0.99531	0.99325	0.98985	0.99571	0.99604	0.99619	0.99633
18	0.99747	0.99686	0.99561	0.99760	0.99768	0.99763	0.99776
Average	0.99727	0.99651	0.99496	0.99742	0.99758	0.99768	0.99764

nature images captured by color sensors. Table 2 shows the selected images from LC dataset for the subjective image quality evaluation.

The objective performance can be assessed using image quality metrics (IQMs) such as color peak signal-to-noise ratio (CPSNR) [14], feature similarity index measure for color images (FSIMc) [19], S-CIELAB ΔE^* [20], zipper effect ratio (ZER) [11], and CPU time. We also present the performance of the proposed algorithm by the subjective image quality comparison.

Our experiments were conducted on an Intel Core i7-8700K CPU @ 3.70GHz with MATLAB R2018a. Experiments of the reference algorithms used the MATLAB code published by the authors. For the subjective image quality evaluation, we used EIZO's ColorEdge CG277 display monitor, which is a professional flagship monitor with self-calibration function providing stable brightness and high color uniformity.

A. OBJECTIVE PERFORMANCE ANALYSIS

The objective performance results evaluated with the five IQMs are listed in Tables 3-7. Table 3 shows that the CPSNR

TABLE 5. S-CIELAB ΔE^* results of conventional algorithms and proposed algorithm for McM dataset.

ΔE^*	VCD	EDUSC	ESF	EDAEP	CDDFW	VDI	Proposed
1	2.9735	4.5958	4.8418	2.9348	3.0127	2.5688	2.6545
2	1.2421	1.8616	1.9255	1.2423	1.3306	1.1363	1.1620
3	2.2113	2.1941	2.5957	2.1648	2.1962	1.6612	1.7813
4	1.3397	1.5828	1.9685	1.3922	1.5403	0.9688	1.0249
5	1.5261	1.9273	2.2893	1.5084	1.5405	1.2900	1.3037
6	1.3262	2.0753	2.8210	1.3217	1.3410	1.0779	1.1337
7	1.0803	0.9459	0.9914	1.1378	1.0351	1.2653	1.2428
8	0.6564	0.7973	0.8633	0.7015	0.6561	0.6623	0.6800
9	1.3476	1.7343	1.9236	1.3227	1.4093	1.0372	1.0754
10	0.9897	1.3014	1.5768	0.9853	1.0138	0.8776	0.8689
11	0.7573	1.0182	1.1574	0.7459	0.7673	0.6658	0.6967
12	1.0070	1.3499	1.5455	0.9398	1.0456	0.9670	0.9166
13	0.7030	0.8585	0.8945	0.6872	0.7113	0.6335	0.6132
14	0.8002	0.9643	1.0862	0.7813	0.7778	0.7080	0.7260
15	0.8553	0.9917	1.1354	0.8258	0.8496	0.7794	0.7445
16	1.8666	2.8537	3.4715	1.8599	1.9080	1.5988	1.7447
17	2.3130	3.6456	3.9487	2.2848	2.5013	1.8305	2.0152
18	1.4655	2.0581	2.1665	1.4813	1.5793	1.4008	1.3496
Average	1.3590	1.8198	2.0668	1.3510	1.4009	1.1738	1.2074

TABLE 6. ZER results of conventional algorithms and proposed algorithm for McM dataset.

ZER	VCD	EDUSC	ESF	EDAEP	CDDFW	VDI	Proposed
1	0.3120	0.3031	0.3815	0.3255	0.3055	0.3028	0.3043
2	0.1999	0.1838	0.2358	0.1995	0.1868	0.1782	0.1777
3	0.1201	0.1208	0.1573	0.1159	0.1244	0.1349	0.1247
4	0.0169	0.0135	0.0292	0.0147	0.0295	0.0230	0.0302
5	0.1014	0.0786	0.1079	0.0997	0.0952	0.0849	0.0875
6	0.0628	0.0661	0.0932	0.0609	0.0508	0.0438	0.0481
7	0.0217	0.0167	0.0240	0.0206	0.0214	0.0313	0.0348
8	0.0383	0.0338	0.0380	0.0378	0.0344	0.0455	0.0509
9	0.1532	0.1540	0.2026	0.1510	0.1472	0.1313	0.1259
10	0.1223	0.1278	0.1611	0.1242	0.1165	0.1017	0.1066
11	0.1222	0.1444	0.1753	0.1271	0.1204	0.1048	0.1010
12	0.0593	0.0487	0.0853	0.0610	0.0507	0.0481	0.0492
13	0.0268	0.0246	0.0387	0.0261	0.0230	0.0206	0.0183
14	0.1822	0.1732	0.2166	0.1795	0.1761	0.1552	0.1575
15	0.1848	0.1782	0.2284	0.1822	0.1865	0.1573	0.1605
16	0.3385	0.4328	0.4796	0.3576	0.3644	0.3272	0.2689
17	0.3747	0.3804	0.4442	0.3798	0.3659	0.3269	0.3215
18	0.2623	0.2596	0.3123	0.2504	0.2723	0.2510	0.1659
Average	0.1500	0.1522	0.1895	0.1507	0.1484	0.1371	0.1296

performance of the proposed demosaicking system is impressive. The average CPSNR of the proposed algorithm is 0.0084-1.9152 dB higher than that of the other algorithms. However, as the CPSNR is an evaluation metric defined through the mean squared error without considering the HVS characteristics, the evaluation using HVS-based metrics must be accompanied.

Tables 4 and 5 present the results using the FSIMc, which is a low-level feature similarity measurement IQM, and S-CIELAB ΔE^* that measures color reproduction errors of digital images. As the FSIMc evaluation result of the proposed algorithm is close to 1, it can be confirmed that the structural characteristics of the resultant image and the original image are very similar. Moreover, the smaller S-CIELAB ΔE^* is, the more similar the color information characteristics of two images are.

Table 6 shows ZER generated in the CFA interpolation process. ZER experimental results show that zipper artifacts are reduced by adopting a post-processing of detecting and eliminating the on-off pattern. Compared with the CPSNR

TABLE 7. CPU time results (s) of conventional algorithms and proposed algorithm for McM dataset.

CPU Time	VCD	EDUSC	ESF	EDAEP	CDDFW	VDI	Proposed
Average	0.2159	0.5577	1.6835	0.1254	0.3503	0.0701	0.2628

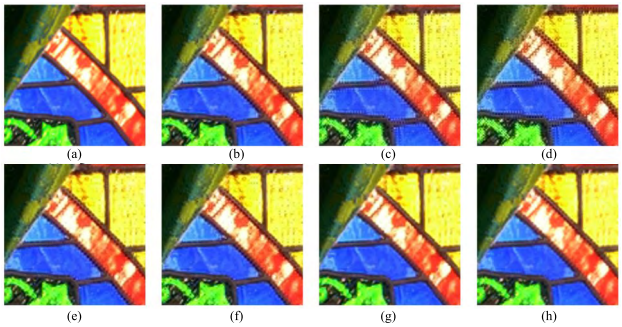

FIGURE 8. Comparison of (a) original image and results of the (b) VCD, (c) EDUSC, (d) ESF, (e) EDAEP, (f) CDDFW, (g) VDI, and (h) Proposed methods (McM #1).

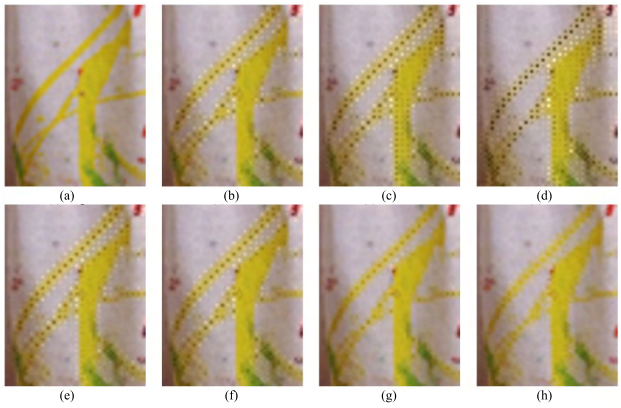

FIGURE 9. Comparison of (a) original image and results of the (b) VCD, (c) EDUSC, (d) ESF, (e) EDAEP, (f) CDDFW, (g) VDI, and (h) Proposed methods (McM #5).

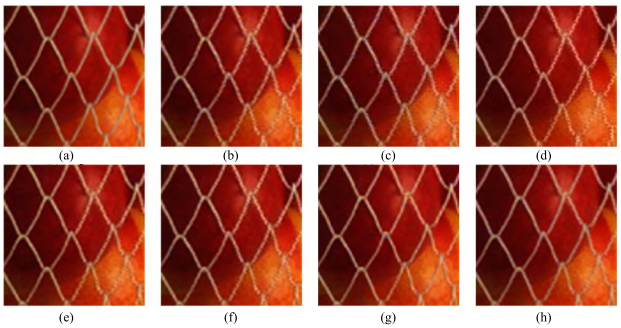

FIGURE 10. Comparison of (a) original image and results of the (b) VCD, (c) EDUSC, (d) ESF, (e) EDAEP, (f) CDDFW, (g) VDI, and (h) Proposed methods (McM #12).

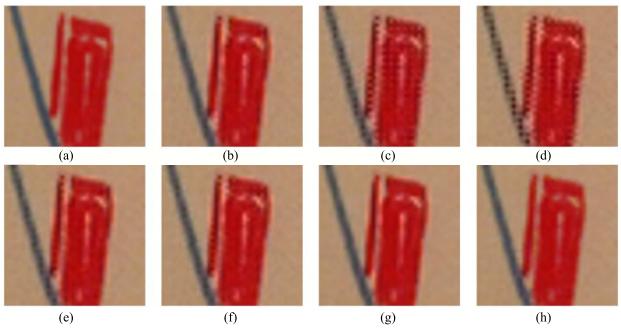

FIGURE 11. Comparison of (a) original image and results of the (b) VCD, (c) EDUSC, (d) ESF, (e) EDAEP, (f) CDDFW, (g) VDI, and (h) Proposed methods (McM #13).

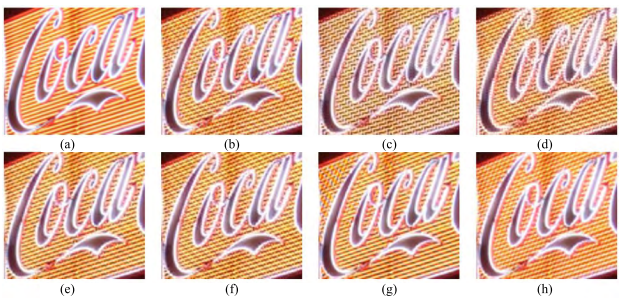

FIGURE 12. Comparison of (a) original image and result of the (b) VCD, (c) EDUSC, (d) ESF, (e) EDAEP, (f) CDDFW, (g) VDI, and (h) Proposed methods (LC #1-1).

results in Table 3, it is seen that lower ZER indicates higher CPSNR. Thus, the post-processing for removing the zipper artifacts is essential to improve the image quality.

Finally, Table 7 shows the average CPU execution time. We can confirm that the proposed algorithm has moderate complexity compared to other algorithms except VDI [10]. Proposed algorithm produced images that are more similar to the original images, with an execution speed that is approximately 6.4060 times faster than ESF. It is expected that a better algorithm will be created by combining low-complexity and high-performance algorithms such as VDI [10] and the post-processing proposed in this paper.

B. SUBJECTIVE PERFORMANCE ANALYSIS

Figs. 8-11 present a subjective image comparison of the demosaicked images of McM images. Each figure shows the experimental results of demosaicking algorithms for McM #1, #5, #12, and #13. It is seen that the proposed algorithm has an overall superior performance. In particular, the results of McM #5 in Fig. 9 and McM #13 in Fig. 11, which contain areas with high saturation values, are excellent. The on-off pattern artifacts that occurred on the yellow line and the red chimney, and the resulting false colors were successfully removed. In Figs. 8 and 10, which is the result for the cropped McM #1 and #12 image, the proposed algorithm shows the most similar results to the original image. On the other hand, other algorithms suffer from false colors caused by zipper artifacts on red and white thin lines.

Figs. 12-14 present a subjective image comparison of the demosaicked images of LC images. Each figure shows the experimental results of demosaicking algorithms for LC #1,

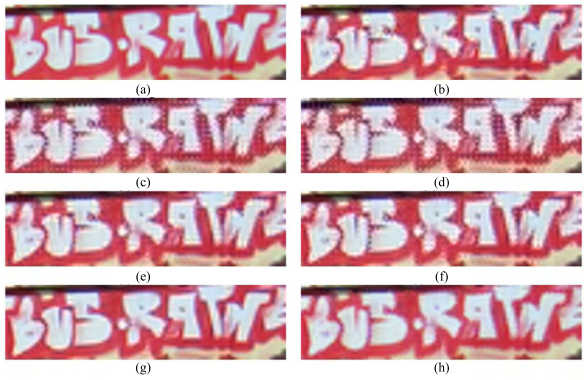

FIGURE 13. Comparison of (a) original image and result of the (b) VCD, (c) EDUSC, (d) ESF, (e) EDAEP, (f) CDDFW, (g) VDI, and (h) Proposed methods (LC #2).

FIGURE 14. Comparison of (a) original image and result of the (b) VCD, (c) EDUSC, (d) ESF, (e) EDAEP, (f) CDDFW, (g) VDI, and (h) Proposed methods (LC #3).

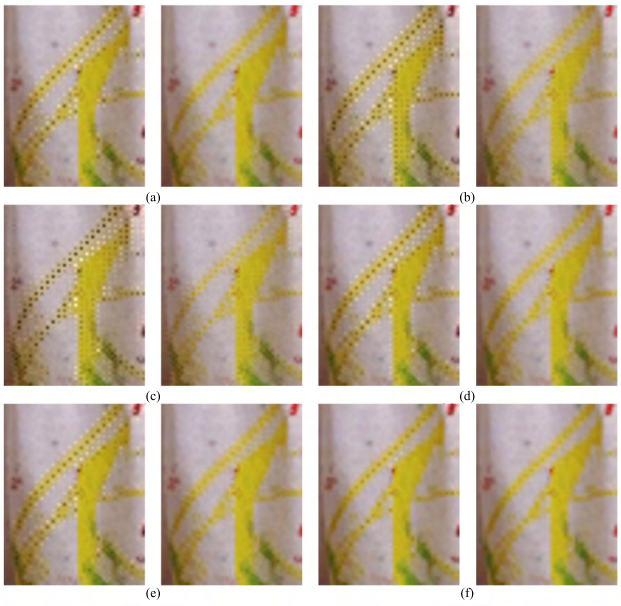

FIGURE 15. Demosaicked image and post-processed image of (a) VCD (b) EDUSC, (c) ESF, (d) EDAEP, (e) CDDFW, and (f) VDI methods (McM #5-1).

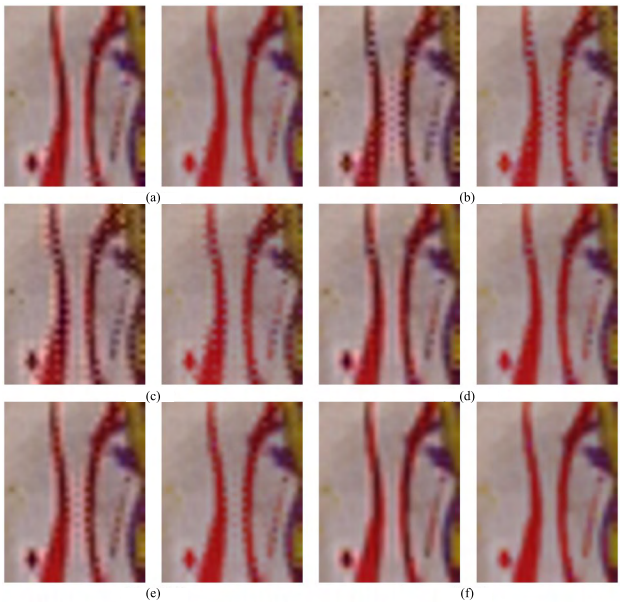

FIGURE 16. Demosaicked image and post-processed image of (a) VCD (b) EDUSC, (c) ESF, (d) EDAEP, (e) CDDFW, and (f) VDI methods (McM #5-2).

#2, and #3. As shown in Fig. 12, the result of the proposed algorithm shows the red color most similar to the original. In particular, the result image of EDUSC in Fig. 12(c) can be confirmed that the edge direction selection is wrong and the pattern is disturbed. In the case of VDI with good results in McM dataset, we can see that rainbow artifacts, as shown in Fig. 12(g). Figs. 13 and 14 show that zipper artifacts are generated from the results of the remaining algorithms except for the VDI and the proposed algorithm, which gives the viewer a bad image quality. In addition, it can be seen that the black color is mixed in the boundary of the object in other algorithms except the proposed algorithm.

Figs. 15-17 illustrate the results of applying the proposed post-processing to the existing demosaicking algorithms. In the case of EDUSC and ESF results of Figs. 16 and 17, in which the image information is greatly lost because of extreme zipper artifacts, it was possible to remove on-off patterns and false colors.

In order to demonstrate the performance of the artifact removal process proposed in this paper, we compared it with AHD [12] which applies median filtering to color differences and HOI [13] which applies a weighted median filtering in the interpolation process. Figs. 18-21 present a subjective image comparison of the images on which artifact removal has been

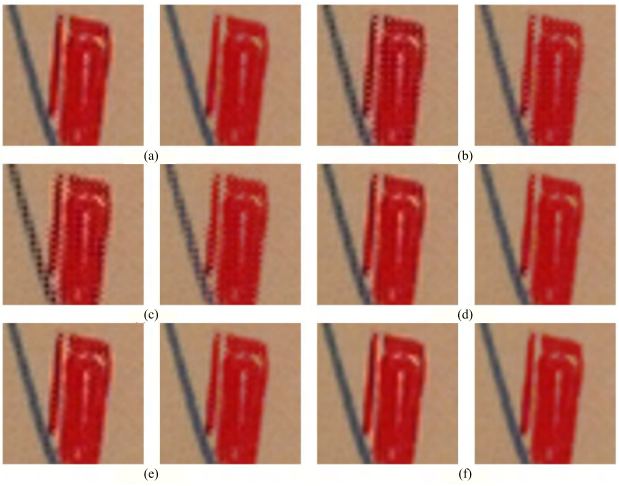

FIGURE 17. Demosaicked image and post-processed image of (a) VCD (b) EDUSC, (c) ESF, (d) EDAEP, (e) CDDFW, and (f) VDI methods (McM #13).

FIGURE 18. Comparison of (a) original image and result of the (b) AHD, (c) HOI, and (h) Proposed methods (LC #1-2).

performed using post-processing. In Figs. 18-21, (a) shows the original image, (b), (c), and (d) show the resulting images of AHD, HOI, and the proposed algorithm, respectively.

FIGURE 19. Comparison of (a) original image and result of the (b) AHD, (c) HOI, and (h) Proposed methods (LC #4).

FIGURE 20. Comparison of (a) original image and result of the (b) AHD, (c) HOI, and (h) Proposed methods (LC #5).

The methods using median filtering are not as good as the proposed post-processing. Figs. 18(b) and (c) show zipper artifacts or false colors in areas with high saturation values, despite median filtering applied. On the other hand, when clamping-based post-processing is performed, as shown in Fig. 18(d), demosaicking artifacts are removed. Similar results can be analyzed in Figs. 19-21.

As can be seen from the various experimental results, the proposed demosaicking system has adavantages. First, it has high interpolation accuracy through the second-order Taylor approximation. Next, it effectively removes the demosaicking artifacts that occur due to the use of a large interpolation kernel. Finally, JND model-based artifact detection and clamping-based artifact removal method is more effective

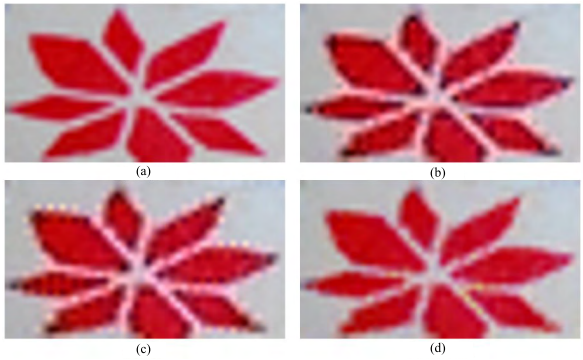

FIGURE 21. Comparison of (a) original image and result of the (b) AHD, (c) HOI, and (h) Proposed methods (LC #6).

than median filtering and can be easily adopted to other interpolation algorithms because it has a separate structure from the demosaicking process.

V. CONCLUSION

In this paper, we proposed a new demosaicking system using quadratic Taylor approximation interpolation and post-processing that can detect and remove demosaicking artifacts. We performed zipper artifact detection based on the JND model using the spatial resolution information of the demosaicked image and obtained the artifact-free image using a clamping-based artifact removal method. As demonstrated in the objective and subjective experimental results, our proposed demosaicking system presents superior performance compared to the conventional demosaicking algorithms.

ACKNOWLEDGMENT

This work was supported by the ICT R&D program of MSIP/IITP (2014-0-00670, Software Platform for ICT Equipment).

REFERENCES

[1] R. Kimmel, "Demosaicing: Image reconstruction from color CCD samples," *IEEE Trans. Image Process.*, vol. 8, no. 9, pp. 1221–1228, Sep. 1999.
[2] D. Alleysson, S. Süsstrunk, and J. Hérault, "Linear demosaicing inspired by the human visual system," *IEEE Trans. Image Process.*, vol. 14, no. 4, pp. 439–449, Apr. 2005.
[3] B. E. Bayer, "Color imaging array," U.S. Patent 3 971 065, Jul. 20, 1976.
[4] B. K. Gunturk, J. Glotzbach, Y. Altunbasak, R. W. Schafer, and R. M. Mersereau, "Demosaicking: Color filter array interpolation," *IEEE Signal Process. Mag.*, vol. 22, no. 1, pp. 44–54, Jan. 2005.
[5] K.-H. Chung and Y.-H. Chan, "Color demosaicing using variance of color differences," *IEEE Trans. Image Process.*, vol. 15, no. 10, pp. 2944–2955, Oct. 2006.
[6] C.-Y. Su and W.-C. Kao, "Effective demosaicing using subband correlation," *IEEE Trans. Consum. Electron.*, vol. 55, no. 1, pp. 199–204, Feb. 2009.
[7] I. Pekkucuksen and Y. Altunbasak, "Edge strength filter based color filter array interpolation," *IEEE Trans. Image Process.*, vol. 21, no. 1, pp. 393–397, Jan. 2012.
[8] W.-J. Chen and P.-Y. Chang, "Effective demosaicking algorithm based on edge property for color filter arrays," *Digital Signal Process.*, vol. 22, no. 1, pp. 163–169, Jan. 2012.
[9] Z. Dengwen, S. Xiaoliu, and D. Weiming, "Colour demosaicking with directional filtering and weighting," *IET Image Process.*, vol. 6, no. 8, pp. 1084–1092, Nov. 2012.
[10] X. Chen, G. Jeon, and J. Jeong, "Voting-based directional interpolation method and its application to still color image demosaicking," *IEEE Trans. Circuits Syst. Video Technol.*, vol. 24, no. 2, pp. 255–262, Feb. 2014.
[11] W. Lu and Y.-P. Tan, "Color filter array demosaicking: New method and performance measures," *IEEE Trans. Image Process.*, vol. 12, no. 10, pp. 1194–1210, Oct. 2003.
[12] K. Hirakawa and T. W. Parks, "Adaptive homogeneity-directed demosaicing algorithm," *IEEE Trans. Image Process.*, vol. 14, no. 3, pp. 360–369, Mar. 2005.
[13] J. S. J. Li and S. Randhawa, "Color filter array demosaicking using high-order interpolation techniques with a weighted median filter for sharp color edge preservation," *IEEE Trans. Image Process.*, vol. 18, no. 9, pp. 1946–1957, Sep. 2009.
[14] D. Menon and G. Calvagno, "Color image demosaicking: An overview," *Signal Process., Image Commun.*, vol. 26, nos. 8–9, pp. 518–533, Oct. 2011.
[15] X. K. Yang, W. S. Ling, Z. K. Lu, E. P. Ong, and S. S. Yao, "Just noticeable distortion model and its applications in video coding," *Signal Process., Image Commun.*, vol. 20, no. 7, pp. 662–680, Aug. 2005.
[16] W. Yin, D. Goldfarb, and S. Osher, "Total variation-based image cartoon-texture decomposition," Columbia Univ., New York, NY, USA, Tech. Rep. CORC Rep. TR-2005-01, UCLA CAM 0527, 2005.
[17] L. Zhang, X. Wu, A. Buades, and X. Li, "Color demosaicking by local directional interpolation and nonlocal adaptive thresholding," *J. Electron. Imag.*, vol. 20, no. 2, p. 023016, Apr. 2011.
[18] L. Condat. (2010). *Image Available*. [Online]. Available: http://www.gipsa-lab.grenoble-inp.fr/~laurent.condat/imagebase.html
[19] L. Zhang, L. Zhang, X. Mou, and D. Zhang, "FSIM: A feature similarity index for image quality assessment," *IEEE Trans. Image Process.*, vol. 20, no. 8, pp. 2378–2386, Aug. 2011.
[20] X. Zhang and B. A. Wandell, "A spatial extension of CIELAB for digital color-image reproduction," *J. Soc. Inf. Display*, vol. 5, no. 1, pp. 61–63, Mar. 1997.

DAEJUN PARK received the B.S. degree from the Department of Electronics and Computer Engineering, Hanyang University, Seoul, South Korea, in 2011, where he is currently pursuing the Ph.D. degree with the Department of Electronics Engineering. His research interests include digital signal processing, image interpolation, image processing, high dynamic range imaging, and HDR/WCG video compression.

JECHANG JEONG received the B.S. degree in electronic engineering from Seoul National University, Seoul, South Korea, in 1980, the M.S. degree in electrical and electronic engineering from the Korea Advanced Institute of Science and Technology, Daejeon, South Korea, in 1982, and the Ph.D. degree in electrical engineering from the University of Michigan, Ann Arbor, MI, USA, in 1990. From 1982 to 1986, he was with the Korean Broadcasting System, where he helped develop teletext systems. From 1990 to 1991, he was a Post-Doctoral Research Associate at the University of Michigan, where he helped to develop various signal processing algorithms. From 1991 to 1995, he was with Samsung Electronics Company, South Korea, where he was involved in the development of HDTV, digital broadcasting receivers, and other multimedia systems. Since 1995, he has conducted research at Hanyang University, Seoul, South Korea. His research interests include digital signal processing, digital communication, and image and audio compression for HDTV and multimedia applications. He has published numerous technical papers. He was a recipient of the Scientist of the Month Award in 1998 from the Ministry of Science and Technology of Korea, the 2007 IEEE Chester Sall Award, and the 2008 ETRI Journal Paper Award. He was also honored with a government commendation in 1998 from the Ministry of Information and Communication of Korea.